ACS APPLIED MATERIALS & INTERFACES

Research Article

www.acsami.org

Effect of Thickness-Dependent Microstructure on the Out-of-Plane Hole Mobility in Poly(3-Hexylthiophene) Films

Bingyuan Huang,[†] Emmanouil Glynos,[†] Bradley Frieberg,[‡] Hengxi Yang,[⊥] and Peter F. Green*[,†,‡,§]

[†]Department of Materials Science and Engineering, [‡]Macromolecular Science and Engineering, [§]Applied Physics, [⊥]Department of Physics, University of Michigan, Ann Arbor, Michigan 48109, United States

Supporting Information

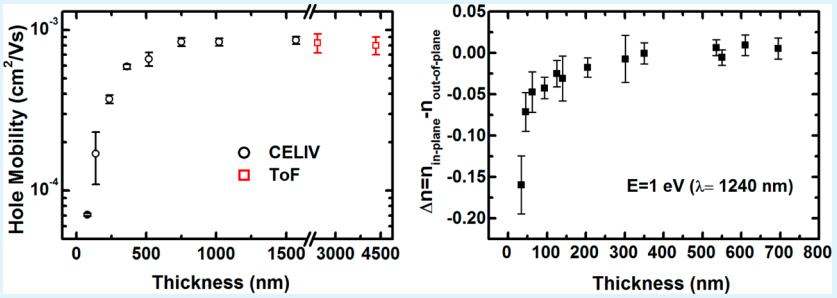

ABSTRACT: Regioregular poly(3-hexylthiophene) (RR-P3HT) is a widely used donor material for bulk heterojunction polymer solar cells. While much is known about the structure and properties of RR-P3HT films, important questions regarding hole mobilities in this material remain unresolved. Measurements of the out-of-plane hole mobilities, μ, of RR-P3HT films have been restricted to films in the thickness regime on the order of micrometers, beyond that generally used in solar cells, where the film thicknesses are typically 100 to 200 nm. Studies of in-plane carrier mobilities have been conducted in thinner films, in the thickness range 100−200 nm. However, the in-plane and out-of-plane hole mobilities in RR-P3HT can be significantly different. We show here that the out-of-plane hole mobilities in neat RR-P3HT films increase by an order of magnitude, from 10^{-4} cm^2/V·s, for a 80 nm thick film, to a value of 10^{-3} cm^2/V·s for films thicker than 700 nm. Through a combination of morphological characterization and simulations, we show that the thickness dependent mobilities are not only associated with the differences between the average morphologies of thick films and thin films, but specifically associated with changes in the local morphology of films as a function of distance from the interfaces.

KEYWORDS: *poly(3-hexylthiophene), mobility, thickness dependence, disordered semiconductors, conjugated polymers, polymer photovoltaic devices*

1. INTRODUCTION

Conjugated polymers are of significant interest for various solid state electronic devices that include field-effect transistors (FETs), light emitting diodes (LEDs), and solar cells.[1−4] Benefits of organic materials for devices include cost-effective and low-temperature processing strategies such as spin coating, drop casting, inkjet printing, and roll-to-roll manufacturing.[5] However, compared to their inorganic counterparts, such as silicon and germanium, limitations of conjugated polymers include intrinsically low charge carrier mobilities, associated with the effects of chemical bonding rendering the carrier transport to occur via hopping among highly localized sites.

The charge carrier mobility impacts the performance of electronic devices in different ways. In organic LEDs, the imbalance between hole and electron mobilities in the recombination layer is responsible for charge build-up and impairs the external quantum efficiency.[6] In polymer FETs, inherently low charge carrier mobility restricts switching speeds.[7] In solar cells, the short circuit current, the fill factor, and, consequently, the power conversion efficiency are also affected by charge carrier mobilities.[3,8,9] Therefore, accurate characterization of the carrier mobilities and an understanding of the connection between carrier mobility and morphology are important for both scientific and technological reasons.[10−13]

One conjugated polymer of significant scientific and technological interest is regioregular poly(3-hexylthiophene) (RR-P3HT). This polymer has been widely used in FETs and solar cells,[14−16] due largely to its relatively high hole mobilities, for organics, reported to be as high as 0.1 cm^2/V·s,[17] and excellent solvent processability.[18] Such high hole mobilities originate from the self-assembled lamellar structure of polymer chains in thin films.

In thin films, RR-P3HT forms a semicrystalline structure. In the crystalline phase, the backbones of the chains, of this planar shaped macromolecule, self-organize to form layers, each of which stacks in the $\pi-\pi$ coupling direction to create a lamellar

Received: June 21, 2012
Accepted: September 6, 2012
Published: September 6, 2012

   dx.doi.org/10.1021/am3011252 | ACS Appl. Mater. Interfaces 2012, 4, 5204−5210

structure. The $\pi-\pi$ coupling direction is orthogonal to the alkyl chain stacking direction and the strong $\pi-\pi$ conjugation gives rise to much higher hole mobilities.[17] The lamellae possess edge-on orientations with respect to the substrate when the $\pi-\pi$ coupling direction is parallel to the substrate. When the $\pi-\pi$ coupling direction is perpendicular to the substrate, the lamellae are oriented face-on to the substrate. Hole mobilities are much lower in the direction normal to the substrate than in the direction parallel to the substrate, where the lamellae are oriented edge-on.

Generally, the absolute hole mobilities in RR-P3HT thin films depend on factors that include molecular weight,[19,20] solvent processing conditions,[16] and annealing conditions.[21] Measurements of transport properties in thin film FETs reveal an effect of film thickness on the *in-plane* hole mobility (transport direction parallel to the substrate) of RR-P3HT.[22−25] In the film thickness range from 20 to 200 nm, Gburek and co-authors reported an order of magnitude increase in the hole mobility; they attributed the trend to the improved ordering in thicker films.[24] However, using the same transistor structure, Reséndiz and collaborators reported only a slight decrease in the mobility within the same thickness range.[25] While this difference may be associated with differences between the morphological structures of the films, the issue remains unsolved.

With regard to the operation of solar cells, information about the *out-of-plane* hole mobility (transport direction normal to the substrate) is more relevant than the in-plane mobility, as the effective charge extraction occurs normal to the substrate in the bulk heterojunction device structure. The out-of-plane mobility is generally very different from in-plane mobility due to the anisotropy of crystalline RR-P3HT.[17] Typically, the out-of-plane hole mobility of high regioregularity P3HT is reported to be within the range of $10^{-4}-10^{-3}$ $cm^2/V{\cdot}s$, measured using the time-of-flight (ToF) measurement technique; no evidence of a film thickness dependence has been reported.[13,19,26,27] However, these ToF measurements of the out-of-plane mobilities were performed on films in the thickness range of micrometers; out-of-plane hole mobility data for thinner conjugated polymer films are difficult to find. The effect of a substrate on the morphology of conjugated polymers is particularly important in thin films, in the thickness range of tens of nanometers. The out-of-plane carrier mobilities would be expected to be thickness dependent in this thickness regime. This issue has remained largely unexplored.

To this end, we report a study of the out-of-plane hole mobilities in RR-P3HT films, with thicknesses from 80 nm to over 1 μm, using the methods of charge extraction by linearly increasing voltage (CELIV) and ToF. Surprisingly, the hole mobilities were lowest in the thinnest films, and increased by over an order of magnitude in films of thickness greater than 700 nm; the mobilities remained constant for thicker films. We show that this behavior is connected to changes in the morphology, characterized using grazing incidence X-ray diffraction (GIXRD) and spectroscopic ellipsometry (SE), of the film, associated with effects of the underlying substrate.

2. EXPERIMENTAL SECTION

Sample Preparation. The samples were prepared using the following procedures. A layer of poly(3,4-ethylenedioxythiophene)-poly(styrenesulfonate) (PEDOT:PSS) (Clevios PH 500) was first spin coated onto a precleaned indium tin oxide (ITO) coated glass substrate and then baked at 150 °C for 15 min in a nitrogen environment on a hot plate. Prior to spin coating of PEDOT:PSS, the ITO-coated glass substrates were solvent cleaned by consecutive ultrasonication in DI water, acetone, and isopropanol for 10 min each step and, then, cleaned under ultraviolet light for 10 min.

The RR-P3HT used in our study, as received, was purchased from Rieke Metals Inc.; it is of ∼95% regioregularity and number average molecular weight 50 000 g/mol. The RR-P3HT was dissolved in chlorobenzene, shaken for over 10 hours, and filtered with 0.45 μm Teflon filters. The solution concentrations were varied from 7 to 52 mg/mL so that different film thicknesses could be spin coated, from the chlorobenzene solutions, onto the PEDOT:PSS/ITO substrates. These samples were then thermally annealed at 150 °C for 15 min. Subsequently, 2 nm thick layers of lithium fluoride were evaporated on top of these structures followed by evaporation of a layer of aluminum, serving as the top electrode, through shadow masks, at a typical pressure of 10^{-7} mbar. For the CELIV measurements, the aluminum layer was 100 nm thick, and for the ToF measurements, the aluminum layer was 20 nm thick.

All solution spin-coating and thermal treatments were performed in a glovebox under nitrogen atmosphere (moisture < 5 ppm, oxygen < 5 ppm); the samples were transferred to the evaporation chamber without exposure to the atmosphere.

Hole Mobility Measurements. The ToF and CELIV are well-established techniques and carefully described in a number of publications,[28,29] so we will describe information specific to our experiments. The ToF measurements were performed using a nitrogen laser (VSL337 from Newport) with a wavelength of λ = 337.1 nm, an intensity per pulse of approximately 120 μJ, and a pulse width less than 4 ns, for photogeneration of charge carriers in the films. A Sorensen XHR300 DC power supply was used to apply constant voltage over devices. The current transients were then amplified using a FEMTO DLPCA-200 low noise current amplifier and recorded with a Tektronix TDS3052C digital oscilloscope.

For the CELIV measurements, a BK Precision 4075 function generator was used to apply the increasing voltage to the device to extract current transients. The current transients were then amplified using the FEMTO amplifier and recorded using the Tektronix digital oscilloscope. The ToF measurements were conducted in air while the CELIV measurements were conducted in a cryostat (VPF100 from Janis), which provided a vacuum of approximately 1 mTorr and a wide temperature range. Details of the experimental data and analysis are described later.

Structural Characterization. The crystalline structure of the RR-P3HT thin film was investigated using grazing incidence X-ray diffraction (GIXRD). Characterization was performed with a Rigaku Ultimate IV diffraction spectrometer (Rigaku, Tokyo, Japan) operating at 40 kV and 44 mA with Cu Ka radiation (λ = 1.5418 Å). Careful alignment of source and detector with respect to the sample was achieved by using a thin film attachment with three degrees of freedom. During the GIXRD measurements, the incident angle was fixed at 0.5°, relative to the plane of sample surface. The scanning angle was measured every 0.02° at rate of 0.5°/min in the out-of-plane direction.

The thicknesses were measured using atomic force microscopy (AFM), and optical properties of RR-P3HT were measured using a variable angle spectroscopic ellipsometer, VASE (M-2000, J.A. Woollam Co.). VASE measurements were performed in the transmission mode and the reflection mode at angles of 55°, 60°, 65°, 70°, and 75°. The film thicknesses and complex refractive indices were measured by fitting the acquired ellipsometric angles Δ and Ψ to a Glass/PEDOT/Cauchy model using two different procedures in the CompleteEASE software (J.A. Woollam Co.). The first was accomplished by measuring films in both transmission mode and reflection mode (transmission weight of 300%),[30] and the second was done through use of multisample analysis (three samples of similar thickness, ±5%).[31] Samples of Glass/PEDOT were also measured to correctly determine the optical properties of PEDOT using a generalized oscillator model (GOM), which were observed to be similar to those found in the literature.[30] A glass/PEDOT/Cauchy model was used to fit to the thickness in the transparent region of RR-

P3HT, with incident light energy less than 1.87 eV (λ > 750 nm). This region was verified to be transparent by the transmission ellipsometry measurements. The optical constants for the entire measured spectrum (0.7–6.5 eV) were then determined by direct inversion of the ellipsometric equations. The resultant optical properties of the RR-P3HT layer were then parametrized to verify that the values were physical and Kramers–Kronig (KK) consistent. The RR-P3HT layer was then confirmed to be anisotropic as has been shown in the literature.[30,31] The degree of anisotropy was determined by the difference between refractive indices in the ordinary and extra-ordinary directions, i.e., the in-plane and out-of-plane directions respectively ($\Delta n = n_o - n_e$).[31] For our study, the degree of anisotropy was evaluated at an incident energy of 1.00 eV ($\lambda \sim 1240$ nm), well in the transparent region of RR-P3HT. Nevertheless, please note that any wavelength in the transparent region exhibits the same trend.

3. RESULTS AND DISCUSSION

The out-of-plane hole mobilities in RR-P3HT films with thicknesses ranging from 80 nm to 1.5 μm were measured by the CELIV method. Unlike ToF, the CELIV method requires no injection or photoexcitation of charge carriers, so the problem of internal electric field perturbations is avoided. This problem restricts the application of ToF to relatively thick films; the CELIV technique is appropriate for thinner films.[28]

Plotted in Figure 1 are the results from the CELIV measurements of RR-P3HT films; the current densities are

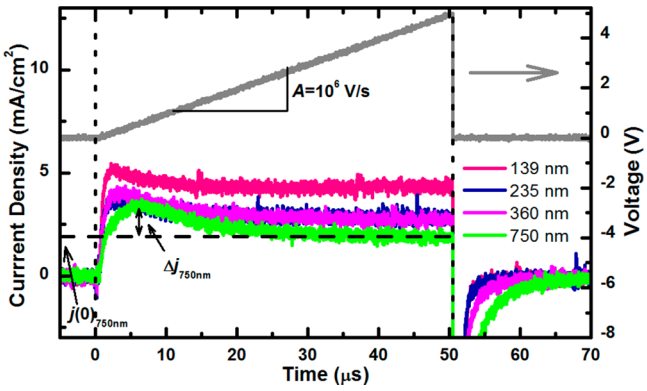

Figure 1. Raw data of CELIV measurements of RR-P3HT films with different thicknesses. The upper curve represents the voltage of a ramping rate of $A = 1 \times 10^6$ V/s. The four lower curves are the current transients extracted from RR-P3HT films. $j(0)$ and Δj for 750 nm film are identified by arrows.

potted as a function of time for four different film thicknesses. The upper curve represents the voltage applied to each sample at room temperature; it ramps up at the rate of $A = 1 \times 10^6$ V/s. Current transients, exhibited by each film, exhibit maxima during the early stages of the application of the electric field. The CELIV model, developed to interpret the data, assumes that the diffusion current is negligible, so the current transient has two major contributions: the displacement current and the drift current.[28] The displacement current $j(0)$ is due to the geometric capacitance of the sample and becomes smaller as the film thickness increases. The drift current, Δj, represents the charges extracted from the film and becomes larger in thicker films because more charges are extracted. The values of the drift and displacement currents in the 750 nm thick film are identified by the arrows in Figure 1. The time at which the total current transient reaches maximum, t_{max}, is measured from the drift current and is used to calculate the hole mobility μ:[28]

$$\mu = \frac{2d^2}{3At_{max}^2\left(1 + 0.36\frac{\Delta j}{j(0)}\right)} \quad (1)$$

where d is the film thickness, A is the voltage ramping rate, and $\Delta j = j(t_{max}) - j(0)$, and $j(0) = A\varepsilon\varepsilon_0/d$, with ε_0 and ε the vacuum permittivity and relative permittivity.

The out-of-plane hole mobilities obtained from the CELIV measurements for seven different RR-P3HT thin films are plotted in Figure 2 (black circles). The mobility increases

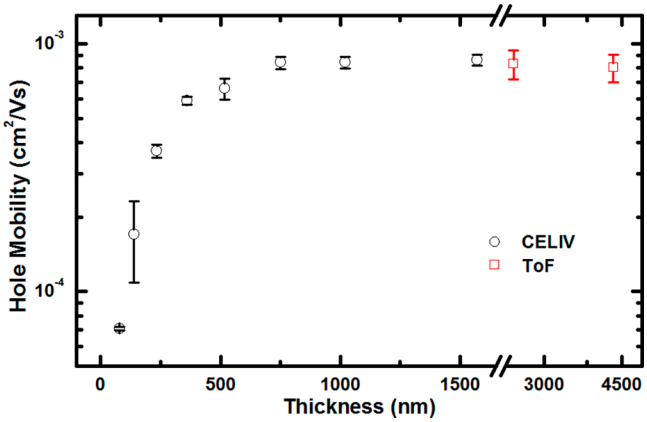

Figure 2. Thickness dependence of hole mobilities measured by both CELIV (black circles) and ToF (red squares) methods displayed on a semilog scale.

monotonically from 7.1×10^{-5} to 8.6×10^{-4} cm^2/V·s as the thickness is increased from 80 to 700 nm and reaches a plateau for thicknesses beyond 700 nm. This thickness dependence, to the best of our knowledge, has not been previously reported. It would not have been measured using ToF because ToF measurements are usually conducted on films with thicknesses typically greater than approximately 1 μm. Our data reveal that for thicknesses greater than 700 nm, the mobility reaches a plateau value of $\mu = 8.6 \times 10^{-4}$ cm^2/V·s. This value is in excellent agreement with those measured using ToF (red squares in Figure 2) for thicker films in the range of 2–5 μm. Before providing an explanation for this thickness dependence in terms of the morphology of the film, we will first discuss the field dependence of the mobilities to show that they are consistent with the theory that describes transport in disordered conductors.

The hole mobility in RR-P3HT films is influenced by the external electric field. In the case of the CELIV measurements, the applied voltage is increased linearly throughout the measurement, so the electric field is not constant. The electric field of interest in our experiments is extracted at the time when the current reaches its maximum value; this specific time is the time used to calculate the carrier mobility. We examined a range of film thicknesses; each film in our study was subjected to various voltage ramping rates. Each transient current maximum value is associated with a ramping rate and a certain electric field. The field dependencies of hole mobilities are plotted in Figure 3. For any specific electric field, the enhancement of the mobility is almost one order of magnitude larger for the 750 nm film, compared to the 80 nm thick samples, as shown in Figure 2. For the 750 nm film, the values we measured for the hole mobilities are in excellent agreement

dx.doi.org/10.1021/am3011252 | ACS Appl. Mater. Interfaces 2012, 4, 5204–5210

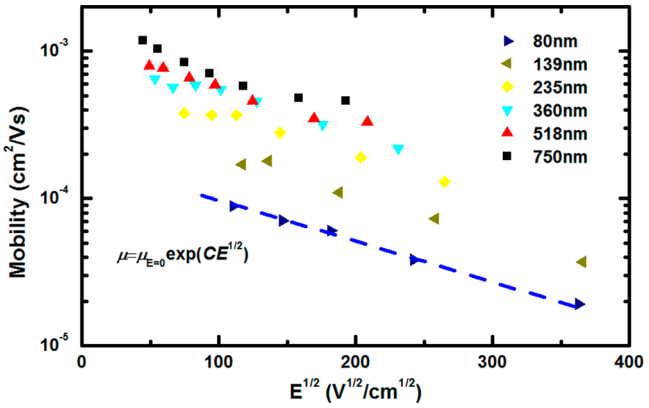

Figure 3. Electric field dependence of out-of-plane hole mobilities in RR-P3HT thin films of increasing thicknesses. The dashed line shows a good agreement between the experimental results and the Poole–Frenkel relationship.

with the results obtained using the ToF technique throughout the entire electric field region.[29]

For each thickness, the electric field dependence of hole mobility is in agreement with the Poole–Frenkel relationship (indicated by the blue dashed line in Figure 3):[26]

$$\mu = \mu_{E=0}\exp(CE^{1/2}) \quad (2)$$

even for electric fields as low as $E = 2.5 \times 10^5$ V/m ($E^{1/2} = 50$ $V^{1/2}/cm^{1/2}$). In this equation $\mu_{E=0}$ is the mobility extrapolated to zero electric field and C is a coefficient. The Poole–Frenkel theory describes the electric-field-assisted thermal motion of charge carriers between localized states in a semiconductor. With increasing electric field, the charge carriers require less thermal energy for delocalization and the mobility increases. This trend has been observed in low molecular weight P3HT thin films before.[32] However, we used high molecular weight P3HT. The data in Figure 3 show that $C < 0$ for all film thicknesses, indicating the mobility decreases with increasing electric field. Such a decrease of the mobility with increasing electric field has been widely reported for high molecular weight RR-P3HT films in this electric field range and for other disordered conductors.[29,33−36] Carrier transport in disordered conductors is influenced by the statistical distribution of energy states and by the spatial distribution of sites (structural disorder) into which the carriers hop. In an environment of significant structural disorder, the effect of the structural disorder is to oppose the long-range transport of the carriers. If the structural disorder has the dominant influence on transport, then $C < 0$ and the mobility would decrease with increasing electric field.

Specifically with regard to RR-P3HT, the hole mobility along the $\pi-\pi$ coupling direction is two orders of magnitude higher than in the transverse direction.[17] Because the RR-P3HT film is composed of crystal domains with different orientations, associated with a distribution of $\pi-\pi$ coupling directions, the hole mobility is influenced by the morphology. So macroscopic carrier transport in RR-P3HT in the presence of a sufficiently large electric field would be impeded by the inherent structure of the material, thereby leading to the decreasing mobility with increasing electric field (i.e.: $C < 0$), as observed here.

The film thickness dependence of the mobility of RR-P3HT may be reconciled in terms of the structure of RR-P3HT thin films. In thin RR-P3HT films, P3HT tends to form a layer of surface induced edge-on crystalline phase on PEDOT:PSS-coated ITO substrate, as shown previously in the literature.[37] Hence, the out-of-plane direction is the lowest $\pi-\pi$ coupling direction, and the hole mobility is comparatively low; recall that the hole mobility along the $\pi-\pi$ coupling direction is two orders of magnitude higher. However, as the film thickness increases, the substrate-induced-orientation effect decreases and a larger fraction of the film structure will possess other orientations. So the effective $\pi-\pi$ coupling along the out-of-plane direction is enhanced, and therefore, the hole mobility would be expected to increase. Beyond the threshold thickness, the distribution of orientations of crystal domains in the RR-P3HT films becomes completely random. Consequently, the mobility should reach a constant value beyond a threshold thickness.

Structural information, gleaned from grazing incidence X-ray diffraction (GIXRD) and ellipsometry, provides more insight into the issue. GIXRD, with the scattering vector in the out-of-plane direction, was performed to characterize the structure of the films. The data in Figure 4 show the average grain sizes,

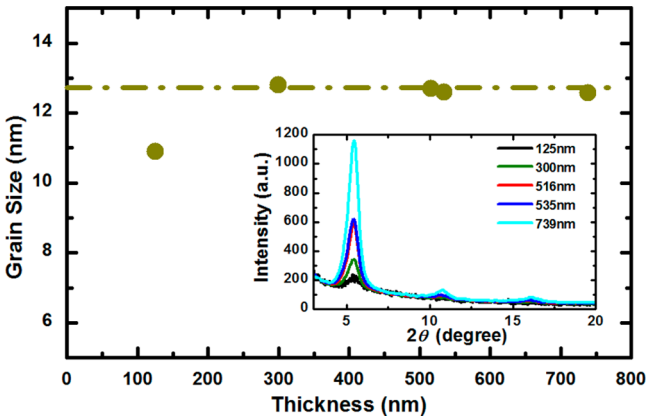

Figure 4. Thickness dependence of grain size in RR-P3HT films. The inset shows raw XRD profiles from which the grain sizes are calculated. The dashed–dotted line indicates where the values saturate.

calculated from the full widths at half-maximum (FWHMs) of the (100) peaks in the profiles (shown in the inset), increased from 10.9 to 12.7 nm; beyond which it remains constant with increasing film thickness. This increase in grain size is in part responsible for the enhancement of the hole mobility; with a larger grain size, the carriers experience fewer crystalline/amorphous/crystalline boundaries to transport as they traverse the film. Carrier mobilities in the amorphous regions are appreciably lower than in the crystalline regions. It is important to note, however, that the grain sizes become constant at thicknesses just less than 300 nm, whereas the carrier mobilities become constant in films that are much thicker, greater than 700 nm. For films thicker than 300 nm, the XRD profiles show no significant change with regard to crystal orientations. The appearance of strong (100) peaks reveals the existence of a significant amount of edge-on crystalline phases in each film. Nevertheless, this cannot exclude the possible existence of face-on crystalline phase because the characteristic (020) peak of face-on phase is centered at $2\theta \approx 21.6°$,[17] which is beyond our current measurement range.

However we show below that a comparable fraction of face-on phases exist in all these films. The different orientations of the edge-on and face-on phases contribute to optical anisotropy

of the film.[31] The degree of optical anisotropy of the films was investigated using VASE. Refractive indices in the ordinary and extra-ordinary directions, which are the in-plane and out-of-plane directions respectively, were determined by fitting the ellipsometric data through a careful procedure previously described by Ng and Campoy-Quiles.[30,31] The degree of anisotropy was then determined from the difference of these two indices, as shown in Figure 5, as a function of film

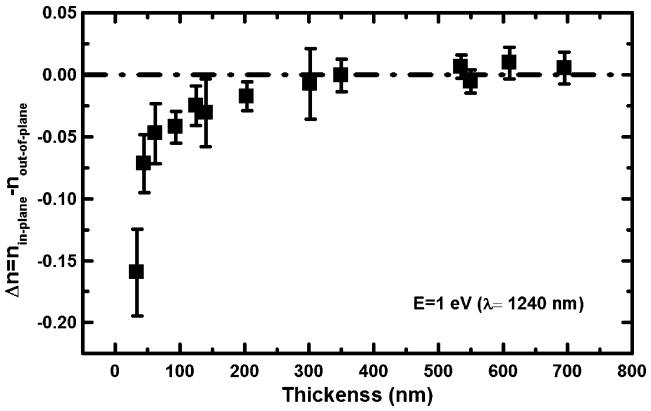

Figure 5. Difference between the in-plane and out-of-plane refractive indices against the film thickness. The dashed−dotted line shows the zero anisotropy level.

thickness. In thin films, the out-of-plane refractive index is larger than the in-plane refractive index, indicating an anisotropic film structure. This is due to the effect of the substrate-induced orientation of edge-on crystals.[37] As the film thickness increases, the difference diminishes and sufficiently far from the interface the two indices become comparable. This implies that the film structure gradually changes from a highly anisotropic state to an isotropic state. Since we have already confirmed the existence of edge-on crystalline phase from the GIXRD, such isotropy indicates that a comparable amount of face-on crystalline phase must also exist in the films, which is favorable to the out-of-plane mobility. Interestingly, the isotropic state begins to develop at about 300 nm from the substrate. This is consistent with the thickness at which grain size becomes constant. We note, however, that this thickness is less than the thickness of 700 nm, beyond which the hole mobilities become constant.

In order to reconcile the different length scales where the transport properties become constant and where the structure becomes isotropic, a simple simulation of the thickness dependence of optical and electric transport properties is carried out on a thin film structure. The film is modeled as a three-dimensional lattice of cubes, with 100 × 100 cubes in the *xy*-plane parallel to the substrate, and the number of layers of cubes in *z*-direction represents the film thickness. Each cube is treated as a crystal domain, which has well defined optical and electric transport properties associated with its orientation with respect to the substrate, indexed from 1 to 10. A value of 1 denotes a completely edge-on configuration, which has the highest resistivity in the out-of-plane direction; a value of 10 denotes a purely face-on configuration, which has the lowest resistivity. The other values denote intermediate cases. The highest resistivity is assumed to be 100 times larger than the lowest one; see the Supporting Information for additional details. To illustrate the substrate effect on crystalline orientations, we created the film such that the first layer is composed of a purely edge-on configuration, identified as Cube 1. The second layer is composed of 90% Cube 1 and 10% randomly assigned cubes. The third layer is 80% Cube 1 and 20% randomly chosen cubes. The subsequent layers are described accordingly; beyond the 11th layer, the structure is completely random. Our system is defined such that the fraction of Cube 1 in the entire film would gradually saturate at 10%.

The anisotropy, represented by the orientation index, is calculated by the arithmetic mean of indices of all cubes for film thickness, in analogy to how ellipsometry averages the optical properties of a film. With regard to the electric transport property, a charge carrier follows a random walk from the first layer to the last through a path determined by a probabilistic criterion (please refer to the Supporting Information for details). The values of resistivities of all cubes in this path are then averaged to generate the conductivity, which can be scaled to a mobility value. For each thickness, 1000 runs were performed and the final mobility was averaged over the 1000 values. Both the anisotropy and mobility data were normalized and plotted in the Figure 6. As the film thickness increases, the

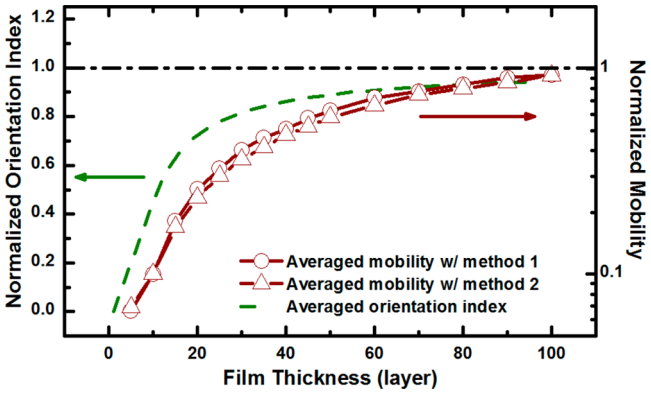

Figure 6. Simulated results of the optical property, which is represented by orientation index, and transport property, which is represented by effective mobility. The dashed−dotted line indicates where the properties saturate. Methods 1 and 2 are discussed in detail in the Supporting Information.

normalized orientation index increases from 0 (completely edge-on, anisotropy) to 1 (completely random, isotropy), which qualitatively reflects the change of film from anisotropic to isotropic, as shown by the ellipsometry data. This trend is consistent with the hole mobility data shown in the figure. Both plateaus are due to the introduction of additional cubes of random orientations in higher-order layers. This reflects the reality that the effect of substrate on the formation of edge-on phase is diminished with distance away from the substrate. Note that, however, the simulated optical property reaches a plateau value for thinner films than the simulated electric transport property. We would like to emphasize here that despite the fact that our simulated results are based on structural change of a 10% gradient per layer, the plateaus and locations of plateaus of the optical and electrical properties are universal for any gradient film microstructure (See the Supporting Information).

As described above, the changes and plateaus in both anisotropy and out-of-plane mobility are due to a substrate-induced gradient in film structure. When the thickness of the

film is small (e.g., 100 nm), this effect is most pronounced. The discrepancy between the onsets of the plateaus predicted by the simulations is due to the different ways of averaging the optical and electric transport properties. The experimentally measured anisotropy, grain size and mobilities are also averaged values and are consistent with the results of the simulations. It is clear that while the average film structure does not change significantly, the average electric transport properties can undergo appreciable changes. These results, from the simulations and the experiments, represent an important step toward understanding the connection between transport properties and the structure. Indeed characterization of the average macroscopic structure may not be sufficient predict the behavior of the macroscopic transport properties. Transport properties are generally influenced by tortuous microscopic pathways within the system.

4. CONCLUSION

In this paper, we studied the thickness dependence of the out-of-plane hole mobility in RR-P3HT thin films ranging in thickness from 80 nm to over 1 μm. The mobility monotonically increased by an order of magnitude as the thickness increased and reached a value of approximately 1×10^{-3} $cm^2/V{\cdot}s$ for thicknesses greater than 700 nm. The implication here is that the carrier mobilities are not constant in this material. At the substrate, the orientation of the molecules is edge-on, and with increasing distance from the substrate, the fraction of the face-on orientation increase. The out-of-plane hole mobilities in the edge-on direction are orders of magnitude slower than in the face-on orientations. Such structural changes are due to a substrate effect, as shown by the ellipsometric measurements of anisotropy and simulations. The increase of the hole mobilities is qualitatively understood from the fact that as the film thickness increases, the structural anisotropy of the film decreases, due to the increase in the fraction of different orientations that favor more rapid out-of-plane carrier transport. Measurements that reflect structural evolution reveal that for film thicknesses greater than 300 nm, the average grain size and anisotropy remains constant. However, the hole mobility continues to increase for films as thick as 700 nm. This difference between locations of plateau values associated structural and electric transport properties is likely associated with the fact that the transport properties are influenced not only by the macroscopic morphology but also by tortuous microscopic pathways.

■ ASSOCIATED CONTENT

Ⓢ Supporting Information

Simulation details of optical and electrical properties of RR-P3HT thin films and results from films with other gradients than 10%. This material is available free of charge via the Internet at http://pubs.acs.org.

■ AUTHOR INFORMATION

Corresponding Author

*E-mail: pfgreen@umich.edu.

Notes

The authors declare no competing financial interest.

■ ACKNOWLEDGMENTS

The authors thank Prof. Barry Dunietz for helpful discussions. This work was supported as part of the Center for Solar and Thermal Energy Conversion, an Energy Frontier Research Center funded by the U.S. Department of Energy, Office of Science, Office of Basic Energy Sciences under Award Number DE-SC0000957.

■ REFERENCES

(1) Facchetti, A. *Mater. Today* **2007**, *10* (3), 28−37.
(2) Kulkarni, A. P.; Tonzola, C. J.; Babel, A.; Jenekhe, S. A. *Chem. Mater.* **2004**, *16* (23), 4556−4573.
(3) Guenes, S.; Neugebauer, H.; Sariciftci, N. S. *Chem. Rev.* **2007**, *107* (4), 1324−1338.
(4) Kroon, R.; Lenes, M.; Hummelen, J. C.; Blom, P. W. M.; de Boer, B. *Polym. Rev.* **2008**, *48* (3), 531−582.
(5) Hoth, C. N.; Schilinsky, P.; Choulis, S. A.; Brabec, C. J. *Nano Lett.* **2008**, *8* (9), 2806−2813.
(6) Giebink, N. C.; Forrest, S. R. *Phys. Rev. B* **2008**, *77* (23), 235215.
(7) Newman, C. R.; Frisbie, C. D.; da Silva Filho, D. A.; Brédas, J.-L.; Ewbank, P. C.; Mann, K. R. *Chem. Mater.* **2004**, *16* (23), 4436−4451.
(8) Schilinsky, P.; Waldauf, C.; Hauch, J.; Brabec, C. J. *J. Appl. Phys.* **2004**, *95* (5), 2816−2819.
(9) Scharber, M. C.; Mühlbacher, D.; Koppe, M.; Denk, P.; Waldauf, C.; Heeger, A. J.; Brabec, C. J. *Adv. Mater.* **2006**, *18* (6), 789−794.
(10) Lebedev, E.; Dittrich, T.; Petrova-Koch, V.; Karg, S.; Brutting, W. *Appl. Phys. Lett.* **1997**, *71* (18), 2686−2688.
(11) Hertel, D.; Bassler, H.; Scherf, U.; Horhold, H. H. *J. Chem. Phys.* **1999**, *110* (18), 9214−9222.
(12) Martens, H. C. F.; Blom, P. W. M.; Schoo, H. F. M. *Phys. Rev. B* **2000**, *61* (11), 7489−7493.
(13) Choulis, S. A.; Kim, Y.; Nelson, J.; Bradley, D. D. C.; Giles, M.; Shkunov, M.; McCulloch, I. *Appl. Phys. Lett.* **2004**, *85* (17), 3890−3892.
(14) Sirringhaus, H.; Tessler, N.; Friend, R. H. *Science* **1998**, *280* (5370), 1741−1744.
(15) Padinger, F.; Rittberger, R. S.; Sariciftci, N. S. *Adv. Funct. Mater.* **2003**, *13* (1), 85−88.
(16) Bao, Z.; Dodabalapur, A.; Lovinger, A. J. *Appl. Phys. Lett.* **1996**, *69* (26), 4108−4110.
(17) Sirringhaus, H.; Brown, P. J.; Friend, R. H.; Nielsen, M. M.; Bechgaard, K.; Langeveld-Voss, B. M. W.; Spiering, A. J. H.; Janssen, R. A. J.; Meijer, E. W.; Herwig, P.; de Leeuw, D. M. *Nature* **1999**, *401* (6754), 685−688.
(18) Hotta, S.; Soga, M.; Sonoda, N. *Synth. Met.* **1988**, *26* (3), 267−279.
(19) Ballantyne, A. M.; Chen, L.; Dane, J.; Hammant, T.; Braun, F. M.; Heeney, M.; Duffy, W.; McCulloch, I.; Bradley, D. D. C.; Nelson, J. *Adv. Funct. Mater.* **2008**, *18* (16), 2373−2380.
(20) Zhang, R.; Li, B.; Iovu, M. C.; Jeffries-El, M.; Sauvé, G.; Cooper, J.; Jia, S.; Tristram-Nagle, S.; Smilgies, D. M.; Lambeth, D. N.; McCullough, R. D.; Kowalewski, T. *J. Am. Chem. Soc.* **2006**, *128* (11), 3480−3481.
(21) Xiao, X.; Wang, Z.; Hu, Z.; He, T. *J. Phys. Chem. B* **2010**, *114* (22), 7452−7460.
(22) Sandberg, H. G. O.; Frey, G. L.; Shkunov, M. N.; Sirringhaus, H.; Friend, R. H.; Nielsen, M. M.; Kumpf, C. *Langmuir* **2002**, *18* (26), 10176−10182.
(23) Wang, G. *J. Appl. Phys.* **2003**, *93* (10), 6137.
(24) Gburek, B.; Wagner, V. *Org. Electron.* **2010**, *11* (5), 814−819.
(25) Reséndiz, L.; Estrada, M.; Cerdeira, A.; Iñiguez, B.; Deen, M. J. *Org. Electron.* **2010**, *11* (12), 1920−1927.
(26) Ballantyne, A. M.; Wilson, J. S.; Nelson, J.; Bradley, D. D. C.; Durrant, J. R.; Heeney, M.; Duffy, W.; McCulloch, I. In TOF mobility measurements in pristine films of P3HT: control of hole injection and influence of film thickness. *Organic Photovoltaics VII*, San Diego, CA, USA; SPIE: San Diego, CA, USA, 2006; p 633408−11.
(27) Malhotra, B. D.; Takashima, W.; Pandey, S. S.; Singhal, R.; Endo, K.; Rikukawa, M.; Kaneto, K. *Jpn. J. Appl. Phys. Part 1−Reg. Pap. Short Notes Rev. Pap.* **1999**, *38* (12A), 6768−6771.

(28) Genevicius, K.; Österbacka, R.; Juska, G.; Arlauskas, K.; Stubb, H. *Thin Solid Films* **2002**, *403*−*404*, 415−418.
(29) Kaneto, K.; Hatae, K.; Nagamatsu, S.; Takashima, W.; Pandey, S. S.; Endo, K.; Rikukawa, M. *Jpn. J. Appl. Phys. Part 2*−*Lett.* **1999**, *38* (10B), L1188−L1190.
(30) Ng, A.; Li, C. H.; Fung, M. K.; Djurišić, A. B.; Zapien, J. A.; Chan, W. K.; Cheung, K. Y.; Wong, W.-Y. *J. Phys. Chem. C* **2010**, *114* (35), 15094−15101.
(31) Campoy-Quiles, M.; Etchegoin, P. G.; Bradley, D. D. C. *Phys. Rev. B* **2005**, *72* (4), 045209.
(32) Goh, C.; Kline, R. J.; McGehee, M. D.; Kadnikova, E. N.; Frechet, J. M. J. *Appl. Phys. Lett.* **2005**, *86* (12), 122110−3.
(33) Takashima, W.; Pandey, S. S.; Endo, T.; Rikukawa, M.; Tanigaki, N.; Yoshida, Y.; Yase, K.; Kaneto, K. *Thin Solid Films* **2001**, *393* (1−2), 334−342.
(34) Mozer, A. J.; Sariciftci, N. S. *Chem. Phys. Lett.* **2004**, *389* (4−6), 438−442.
(35) Borsenberger, P. M. *J. Appl. Phys.* **1990**, *68* (11), 5682−5686.
(36) Van der Auweraer, M.; De Schryver, F. C.; Borsenberger, P. M.; Bässler, H. *Adv. Mater.* **1994**, *6* (3), 199−213.
(37) Kim, J. S.; Park, Y.; Lee, D. Y.; Lee, J. H.; Park, J. H.; Kim, J. K.; Cho, K. *Adv. Funct. Mater.* **2010**, *20* (4), 540−545.